Post-exercise intramuscular O_2 supply is tightly coupled with a higher proximal-to-distal ATP synthesis rate in human tibialis anterior

Authors

L. Heskamp[1], F. Lebbink[1], M.J van Uden[1], M.C. Maas[1], J.A.H.R. Claassen [2], M. Froeling[3], G.J. Kemp[4], A. Boss[1], A. Heerschap[1]

[1]Department of Medical Imaging/Radiology, Radboud university medical center, Nijmegen, The Netherlands

[2]Department of Geriatrics, Radboud university medical center, Nijmegen, The Netherlands

[3]Department of Radiology, University Medical Center Utrecht, Utrecht, The Netherlands

[4] Department of Musculoskeletal and Ageing Science, University of Liverpool, Liverpool, UK

Running title: Spatial variations in skeletal muscle oxidative capacity and O_2 supply

Keywords: skeletal muscle, ^{31}P magnetic resonance spectroscopy, oxidative metabolism, phosphocreatine recovery, magnetic resonance imaging

Table of contents category: Muscle

Author addresses

Linda Heskamp, 6500 HB, linda.heskamp@radboudumc.nl

Franciska Lebbink, 6500 HB, franciskalebbink@gmail.com

Mark van Uden, 6500 HB, m.vanuden@tesladc.nl

Marnix Maas, 6500 HB, marnix.maas@radboudumc.nl

Jurgen Claassen, 6500 HB, jurgen.claassen@radboudumc.nl

Martijn Froeling, 3508 GA, m.froeling@umcutrecht.nl

Graham Kemp, L7 8TX, g.j.kemp@liverpool.ac.uk

Andreas Boss, 6500 HB, andi.boss82@gmail.com

Arend Heerschap, 6500 HB, arend.heerschap@radboudumc.nl

Corresponding author

Linda Heskamp

Radboud University Medical Center, Department of Radiology and Nuclear Medicine

P.O. Box 9101, 6500 HB Nijmegen, The Netherlands

e-mail: linda.heskamp@radboudumc.nl

Key points summary

- The post-exercise recovery of phosphocreatine, a measure of the oxidative capacity of muscles, as assessed by ^{31}P MR spectroscopy, shows a striking increase from distal to proximal along the human tibialis anterior muscle.
- To investigate why this muscle exhibits a greater oxidative capacity proximally, we tested whether the spatial variation in phosphocreatine recovery rate is related to oxygen supply, muscle fiber type or type of exercise.
- We revealed that oxygen supply also increases from distal to proximal along the tibialis anterior, and that it strongly correlated with phosphocreatine recovery. Carnosine level, a surrogate measure for muscle fiber type was not different proximal and distal and type of exercise did not affect the gradient in phosphocreatine recovery rate.
- Taken together, the findings of this study suggest that the post-exercise spatial gradients in oxygen supply and phosphocreatine recovery are driven by a higher intrinsic mitochondrial oxidative capacity proximally.

Abstract

Phosphorus magnetic resonance spectroscopy (^{31}P MRS) of human tibialis anterior (TA) revealed a strong proximo-distal gradient in the post-exercise phosphocreatine (PCr) recovery rate constant (k_{PCr}), a measure of muscle oxidative capacity. The aim of this study was to investigate whether this k_{PCr} gradient is related to O_2 supply, resting phosphorylation potential, muscle fiber type, or type of exercise.

Fifteen male volunteers performed continuous isometric ankle dorsiflexion at 30% maximum force until exhaustion. At multiple locations along the TA, we measured the oxidative PCr resynthesis rate (V_{PCr}=k_{PCr}×PCr-depletion) by ^{31}P MRS, the oxyhemoglobin recovery rate constant (k_{O2Hb}) by near infrared spectroscopy, and muscle perfusion with MR intravoxel incoherent motion imaging. The k_{O2Hb}, k_{PCr}, V_{PCr} and muscle perfusion depended on measurement location (p<0.001, p<0.001, p=0.032 and p=0.003, respectively), all being greater proximally. The k_{O2Hb} and muscle perfusion correlated with k_{PCr} (r=0.956 and r=0.852, respectively) and V_{PCr} (r=0.932 and r=0.985, respectively), the latter reflecting metabolic O_2 consumption.

Resting phosphorylation potential (PCr/inorganic phosphate) was also higher proximally (p<0.001). The surrogate for fiber type, carnosine content measured by ^{1}H MRS, did not differ between distal and proximal TA (p=0.884). Performing intermittent exercise to avoid exercise ischemia, still led to larger k_{PCr} proximally compared to distally (p=0.013).

In conclusion, the spatial k_{PCr} gradient is strongly associated with the spatial variation in O_2 supply. It cannot be explained by exercise induced ischemia nor by fiber type. Our findings suggest it is driven by a higher proximal intrinsic mitochondrial oxidative capacity, apparently to support contractile performance of the TA.

Introduction

Muscle contraction requires energy in the form of ATP, whose production is dominated by oxidative phosphorylation in the mitochondria. In any temporary mismatch between ATP supply and use, such as at the onset of exercise, the phosphocreatine (PCr) energy buffer system comes into play, re-phosphorylating ADP to ATP at the expense of PCr, catalyzed by creatine kinase. When the ATP demand of force-generation ceases, the PCr pool is replenished by oxidative phosphorylation. The post-exercise recovery rate constant of PCr (k_{PCr}), which can be measured using dynamic phosphorus MR spectroscopy (^{31}P MRS), can be interpreted as a correlate and marker of the muscle's oxidative capacity, providing that minimal pH changes occur in the preceding exercise period (Taylor *et al.*, 1983; Meyer, 1988; McCully *et al.*, 1993; Kemp *et al.*, 2015). In numerous studies k_{PCr} varies as expected between trained *vs.* untrained subjects, young *vs.* elderly and healthy subjects *vs.* subjects with mitochondrial myopathies or type II diabetes (Arnold *et al.*, 1985; Phielix *et al.*, 2008; Larsen *et al.*, 2009; Fleischman *et al.*, 2010). Furthermore, k_{PCr} is higher in muscles containing predominantly oxidative type I fibers than in muscles in which glycolytic type II fibers are dominant (Söderlund and Hultman, 1991; M. J. Kushmerick *et al.*, 1992; Yoshida *et al.*, 2013). In all these situations, measures derived from post-exercise PCr recovery kinetics correlate with *ex vivo* measures of mitochondrial function or content (Taylor *et al.*, 1983; Meyer, 1988; McCully *et al.*, 1993; Kemp *et al.*, 2015). In ^{31}P MRS and biopsy studies of mitochondrial function it is conventionally assumed that spatial/anatomical gradients within a single muscle body can be neglected. Strikingly, though, we reported that k_{PCr} does vary within a single muscle: following continuous isometric exercise, k_{PCr} was significantly greater in the proximal part of the tibialis anterior (TA) than in the distal part (Boss *et al.*, 2018).

Despite the dominant effects of mitochondrial activity and content, PCr recovery may also reflect extra-mitochondrial factors (Taylor *et al.*, 1983; Meyer, 1988; McCully *et al.*, 1993; Kemp *et al.*, 2015). The most important of these is perhaps the vascular supply of O_2: PCr recovery can be markedly slowed when O_2 supply is impaired, e.g. in peripheral vascular disease, (Harris *et al.*, 1976; Kemp *et al.*, 2015). Similar influences are seen in normal physiology: in healthy subjects muscle perfusion, measured by MR, correlates with k_{PCr} (Carlier *et al.*, 2006). However, whether this coupling between k_{PCr} and O_2 supply also holds when k_{PCr} varies spatially within a single muscle is unknown.

The first aim of this study was to assess whether processes involved in O_2 supply vary spatially along the TA and to what extent this is related to the spatial gradient of post-exercise PCr recovery. We addressed this by combining ^{31}P MRS with two complementary techniques, near infrared spectroscopy (NIRS) and intravoxel incoherent motion imaging (IVIM). NIRS measures changes in oxyhemoglobin (O_2Hb), which reflects the temporary imbalance between O_2 supply and O_2 use, and IVIM measures parameters that reflect muscle perfusion, which is a main determinant of O_2 supply.

Mitochondrial function also has been related to muscle fiber type and to resting-muscle values of free energy of ATP hydrolysis (or phosphorylation potential) (Meyer, 1988; Söderlund and Hultman, 1991; Schiaffino and Reggiani, 2011; Kemp *et al.*, 2015). Therefore, our second aim was to investigate if these varied along the length of the TA with MRS. While the definitive assessment of fiber type proportions requires biopsy, a conveniently non-invasive surrogate biomarker for fiber types in healthy muscles is carnosine content (C. Harris *et al.*, 1998), which can be measured by ^{1}H MRS (Baguet *et al.*, 2011). The PCr/Pi ratio, a surrogate marker for phosphorylation potential, can readily be obtained from ^{31}P MR spectra of resting muscle (Meyer *et al.*, 1985; Martin J. Kushmerick *et al.*, 1992; Takahashi *et al.*, 1996; Kemp *et al.*, 2015).

Finally, to examine the possibility that the observed k_{PCr} gradient is due to spatial variations in the degree of ischemia caused by continuous isometric exercise, we performed ^{31}P MRS measurements following intermittent isometric exercise, in which muscle perfusion is maintained during the relaxation phase.

Materials and Methods

Ethical approval

This study was conducted according to the principles of the Declaration of Helsinki (version October 2013) and the Medical Research Involving Human Subjects Act (WMO), except for registration in a database. It was approved by the local medical ethical committee CMO Arnhem-Nijmegen (NL60135.091.16 and NL58944.091.16), and prior written informed consent was obtained from all subjects.

Subjects and study design

We recruited 20 healthy male subjects aged 18-35 years with BMI 18-25 kg/m^2. Exclusion criteria were contra-indications for MRI scanning or a history of muscular disease. Of the 20 participants, 15 subjects performed continuous isometric ankle dorsiflexion and 5 subjects performed intermittent isometric ankle dorsiflexion. Daily-life activity was determined for the subjects performing the continuous exercise using a validated questionnaire (Craig *et al.*, 2003).

For the continuous exercise, the subjects underwent two experimental sessions, the first for NIRS and the second for MR measurements (IVIM and ^{31}P MRS). For the intermittent exercise, we conducted only ^{31}P MRS without IVIM and NIRS measurements. The subject's right foot was placed in a custom-built MR compatible ergometer connected to a digital force gauge (Sauter FL 500, Balingen, Germany; figure 1A/B) (Boss *et al.*, 2018). At the start of each session, maximum voluntary contraction (MVC) for ankle dorsiflexion was determined as the best of three attempts. This was followed by 15 minutes rest to allow restoration of resting muscle perfusion and PCr levels. The continuous isometric ankle dorsiflexion exercise was performed at 30% MVC until exhaustion (approximately 2 to 5 minutes), and the intermittent isometric ankle dorsiflexion (frequency: 0.5 Hz) started at 10% MVC and incrementally increased with 10% MVC every 30 seconds until exhaustion (till approximately 60-70% MVC).

Data acquisition

NIRS: Concentration changes in O_2Hb were measured simultaneously at 7 positions along the TA using an 8-channel continuous-wave NIRS system (OxyMon MK III, Artinis Medical System, Elst, The Netherlands). We used three wavelengths (765, 857 and 859 nm) and a 50 Hz sampling frequency. The dependent differential path length factor (DPF), which accounts for the increased distance travelled by the light due to scattering, was set at 4.0 to express the O_2Hb signal in micromol per liter (Ferrari *et al.*, 1992). However, the use of this DPF is only for presentational convenience, because the scattering properties of the tissue are likely to vary along the TA and we have therefore only assessed the kinetics of the O_2Hb signal, and not the amplitude changes. The total muscle coverage was 15 cm, with the 7 positions centered 2.5 cm apart (Figure 1C/D). The transmitter-receiver inter-optode distance was 3 cm, resulting in a measurement depth of ~1.5 cm (McCully and Hamaoka, 2000). Data was acquired during 5 minutes rest, the exercise period, and 15 minutes recovery.

MR measurements: The MR measurements were performed on a 3T MR system (Magnetom PrismaFit, Siemens, Erlangen, Germany). In case of the continuous exercise, the subject performed the exercise twice, first to assess muscle perfusion with IVIM and second to measure the PCr recovery with ^{31}P MRS. The muscle perfusion measurement was performed first because the recovery of perfusion to resting post-exercise values is considerably longer than recovery of ^{31}P metabolite levels. There was at least 45 minutes between the two exercise bouts, this is sufficient time for perfusion and the phosphorous metabolites to recover to pre-exercise values.

IVIM: MR images were acquired with a 15-channel Tx-Rx knee coil. We recorded 9 transversal slices with a diffusion weighted spin-echo sequence using echo-planar imaging (EPI) read-out and SPAIR fat suppression (TR: 2000 ms, TE: 40 ms, FOV: 176 x 176, voxel size 2.75 x 2.75 x 10 mm^3, number of slices: 9, slice gap 11.3 mm, receiver bandwidth 2440Hz/pixel, acquisition time: 1 min 18 s). A total of 13 b-values were obtained (0, 5, 10, 15, 20, 40, 60, 80, 100, 150, 200, 400 and 600 s mm^{-2}) in three orthogonal directions. The slices covered a length of 18.4 cm along the proximo-distal axis (figure 1D). We acquired 4 repetitions of the diffusion weighted scan before the start of the exercise, and 12 repetitions after the exercise.

^{31}P MRS: ^{31}P MR spectra were obtained with a custom-built ^{31}P phased array probe (van Uden *et al.*, 2012; Boss *et al.*, 2018) for signal reception, consisting of 5 individual coil elements (size: 4 x 4.5 cm (estimated measurement depth: ~ 2 cm), total size: 4 x 20 cm, overlap of elements for decoupling, figure 1D). We combined this receive coil with a commercially available ^{1}H/^{31}P birdcage coil (Rapid, Rimpar, Germany) for homogeneous phosphorus excitation. This set-up enabled us to receive free induction decays (FIDs) with a high signal-to-noise ratio (SNR) at 5 positions along the TA. The examination started with the acquisition of anatomical T1 weighted images in resting muscle to verify correct placement of the ^{31}P phased array probe (repetition time (TR): 685 ms, echo time (TE): 12 ms, flip angle (FA): 140°, field of view (FOV): 176 x 176 mm^2, voxel size: 0.92 x 0.92 x 10 mm^3, slice gap 11.3 mm, number of slices: 9, number of averages (NA) = 2, turbo spin-echo factor: 3). If the two fish oil capsules, which are attached at the centre of the two outermost elements of the ^{31}P probe, did not appear directly above the TA, the ^{31}P probe was repositioned. Next, we performed 2D ^{31}P MR imaging in the transversal plane with a gradient echo sequence (center frequency on PCr, TR: 1500 ms, TE: 10 ms, NA: 6, FOV: 176 x 176 mm^2, matrix size: 16x16). A 20 cm thick axial slice covering the TA perpendicular to the coil was selected so that for each coil element a 2D transversal ^{31}P MR

image is obtained of the intersection of its sensitive area and this slice. Thereafter, sequential ^{31}P MR spectra were obtained (TR: 2.06 sec, 48° Ernst angle excitation, ^{1}H-^{31}P NOE enhanced). We collected for each of the 5 coil elements ^{31}P MRS spectra at rest (6 averages per spectrum) to determine PCr/Pi, which was followed by the exercise protocol. The exercise protocol consisted of 1 min rest, the continuous or intermittent isometric exercise until exhaustion, and the recovery period. Throughout this rest, exercise and recovery period ^{31}P MR spectra were continuously recorded, with 2 averages per spectrum, for 20 min 36 s.

*Carnosine: S*ingle voxel ^{1}H MR spectra were acquired during rest with the ^{31}P/^{1}H birdcage coil in 6 of the volunteers using an sLASER sequence for voxel localization (TR = 3000 ms, TE = 33 ms, NA =144, bandwidth 1200 Hz) with and without water suppression. Two voxels of 17x17x60 mm were measured, one in the distal and the other in the proximal part of the muscle, avoiding contamination by subcutaneous fat and the extensor digitorum.

Data processing

Data analysis was performed using Matlab version 2014b (Mathworks, Natick, MA, USA).

NIRS: The O_2Hb signal was filtered with a moving average filter of 10 s to remove high-frequency noise. Next, we selected the recovery part of the O_2Hb signal from end-exercise until the maximum value was reached, and baseline-corrected this by subtracting the end-exercise value. This signal was fitted with a mono-exponential model (Eq 1):

$$[O_2Hb(t)] = [O_2Hb_0] + [\Delta O_2Hb](1 - e^{-k_{O2Hb} \cdot t}) \qquad \textit{(Eq 1)}$$

where k_{O2Hb} is the recovery rate constant, O_2Hb_0 is O_2Hb at the end of exercise and ΔO_2Hb is the recovery value of O_2Hb minus O_2Hb_0.

IVIM: The TA was delineated on 8 slices of the b = 0 s mm^{-2} image using MIPAV (http://mipav.cit.nih.gov) for all 16 diffusion weighted acquisitions to determine the average signal intensity for the TA per slice, b-value and diffusion weighted acquisition. The 9th, most proximal, slice was excluded, because the TA was too small to be accurately delineated there in most cases. For each slice and diffusion-weighted acquisition, the diffusion signal decay was fitted with a bi-exponential model (Eq 2), in two steps (Le Bihan *et al.*, 1988).

$$S_b = S_0' \left((1 - F_p) e^{-bD} + F_p e^{-b \cdot D^*} \right) \qquad \textit{(Eq 2)}$$

The diffusion coefficient (D) was computed by a linear least-squared fit to the log-transformed signal for b-values $\geq$ 200 s mm^{-2} according to Eq 3.

$$\log(S_b) = -Db + \log(S_0'') \qquad \textit{(Eq 3)}$$

Thereafter, the perfusion coefficient (D*), perfusion fraction (F_p) and S_0' were fitted with a non-linear least-squared fit to Eq 2 with b-values from 5 to 600 s mm^{-2} with fixed D. The fitted parameters D, D*, F_p, and the blood flow related parameter $F_p \times D^*$ during rest and recovery were defined as the average over the first 4 and last 11 diffusion-weighted acquisitions, respectively. The first acquisition after exercise was excluded, being often corrupted by motion artefacts.

^{31}P MRS: To assess the ^{31}P signal coming from the TA and the extensor digitorum (ED) the contours of these muscles were delineated on the 5 slices of the T1 weighted anatomical images and overlaid on the ^{31}P images. Thereafter, the sum intensity of the ^{31}P signals for both regions of interest was determined to calculate the relative contribution of the two dorsiflexors to the total ^{31}P signal.

The ^{31}P MR spectra were fitted, after phase correction and frequency alignment, using the AMARES algorithm in JMRUI (Stefan *et al.*, 2009) with Lorentzian line shapes, multiplets for ATP, and a singlet or doublet for Pi, as appropriate. Average PCr/Pi ratios were determined from spectra of the TA per coil element, assuming similar ^{31}P T1 relaxation times distally and proximally. The PCr recovery was fitted with a mono-exponential model (Eq 4).

$$PCr(t) = PCr_0 + \Delta PCr(1 - e^{-k_{PCr} \cdot t}) \qquad \textit{(Eq 4)}$$

where k_{PCr} is the rate constant of PCr recovery, PCr_0 is the PCr level at the end of exercise and ΔPCr is the recovery value of PCr minus PCr_0. The parameter t is the time from the moment of the end of exercise. The relative amount of PCr depletion in exercise was calculated from the fitted values as $\Delta PCr/(\Delta PCr + P_0)$. The end-exercise pH ($pH_{endex}$) was determined from the chemical shift difference between Pi and PCr (Moon and Richards, 1973). In cases where two Pi peaks were fitted at end-exercise, the average pH_{endex} was defined as the average pH of the two pH pools. Furthermore, we estimated the post-exercise PCr resynthesis (V_{PCr}) as $k_{PCr} \times \Delta PCr$, because this directly reflects the initial post-exercise O_2 utilization (Kemp *et al.*, 2015). For this calculation, ΔPCr is expressed in mM using an assumed ATP tissue concentration of 8.2 mM and applying T1 relaxation correction ($T1_{ATP}$ = 5 s, $T1_{PCr}$ = 6.6 s).

Carnosine: Signals for carnosine are observed in water-suppressed ^{1}H MRS spectra at 7 ppm and 8 ppm. To determine the relative tissue concentration, the 8 ppm peak was fitted with a Lorentzian line in jMRUI (version 5.2, http://www.jmrui.eu) and its amplitude was normalized to the amplitude of the water signal from the water-unsuppressed ^{1}H MR spectrum (Naressi *et al.*, 2001; Stefan *et al.*, 2009).

Statistical analysis

We assessed the proximo-distal variation in rest total 31P signal and PCr/Pi and post-exercise k_{O2Hb}, D, $F_p \times D^*$, k_{PCr}, and V_{PCr} along the TA in two ways with IBM SPSS Statistics (version 25, Chicago, IL, USA). First, the most distal position was compared with the most proximal position using a two-sided paired samples t-test for the continuous exercise and a Wilcoxon signed rank test for the intermittent exercise. Second, the dependence of PCr/Pi, k_{O2Hb}, D, $F_p \times D^*$, k_{PCr} and V_{PCr} on the location along the TA was tested with linear and non-linear mixed models to account for intrasubject correlations (locations). For the linear mixed model, we included location as a fixed covariate (*i.e.* $y = \beta_0 + \beta_1 location$), and for the non-linear mixed model we included location and its quadratic term as fixed covariates (*i.e.* $y = \beta_0 + \beta_1 location + \beta_2 location^2$). In both mixed models, the intercept was modelled as a random effect, and the variance components covariance structure was used. In case of the evaluation of k_{PCr}, the pH_{endex} was included as an additional fixed linear covariate with coefficient β_3. All models were fitted using a maximum likelihood (ML) estimation, and the most appropriate model, linear or non-linear, was chosen based on the Bayesian Information Criterion (BIC). The ratio of carnosine to water was compared between the distal and proximal voxel with a two-sided paired samples t-test. Moreover, a Pearson's correlation was used to estimate the association between k_{PCr} and V_{PCr} with k_{O2Hb} and $F_p \times D^*$. As the data for the different measurement locations within a single volunteer show a high dependency, the requirement of the Pearson's correlation that all datapoints must be independent is not met. Therefore, we determined the average values of k_{PCr}, V_{PCr}, k_{O2Hb}, and $F_p \times D^*$ from all volunteers per coil element, optode position or image slice and correlated those average values instead of the individual datapoints. Data are presented as mean ± SD unless stated otherwise.

Results

Subjects

The 15 healthy volunteers that performed a continuous isometric exercise were 26 ± 3 years old with BMI 22.8 ± 1.5 kg m^{-2} (table 1). Their self-reported activity ranged from 4-69 hours per week at various intensities (table 1). The 5 additional volunteers doing intermittent isometric exercise were 31 ± 4 years old with BMI 21.3 ± 1.6 kg m^{-2}. For the continuous exercise, some datasets had to be excluded. Two subjects were excluded from the IVIM analyses because of acquisition problems. Furthermore, 5 subjects were excluded from the ^{31}P MRS analysis: in 3 subjects ^{31}P MRS data was not acquired due to scanner problems, 1 subject showed no detectable PCr drop in two probe elements (possibly due to movement of the coil element towards the tibia) and in 1 subject the PCr recovery data could not be properly fitted with the exponential model because PCr did not recover for E1 and E2 (possible also due to coil movement).

MVC and force during exercise

In the continuous isometric exercise group, MVC was 200 ± 42 N for NIRS assessment and 203 ± 24 N for the MR assessment. During the isometric exercise for the NIRS, IVIM and ^{31}P MRS measurements, the measured force was 28.6% ± 1.1% , 28.9% ± 0.7%, and 28.6% ± 0.8% of MVC and the average time to exhaustion was 296 ± 133 s, 250 ± 103 s, and 145 ± 46 s, respectively. The time to exhaustion during intermittent isometric exercise was 187 ± 4 s.

NIRS

The O_2Hb signal of the NIRS measurement, which reflects the imbalance between O_2 supply and O_2 utilization, was stable during rest and decreased as expected during continuous isometric exercise. After the exercise, the O_2Hb signal recovered, often overshooting to a higher value than baseline (figure 2A). In the typical example presented in figure 2B recoveries of the O_2Hb signal are shown for the different optodes with recovery rate constants, k_{O2Hb}, increasing from distal to proximal. On average over all subjects, k_{O2Hb}, was 5.4 ± 3.8 min^{-1} at the distal optode and 7.8 ± 4.4 min^{-1} at the proximal optode (p = 0.011; table 2, figure 2C).

IVIM

The diffusion-weighted MR images after continuous isometric exercise revealed an increased signal intensity compared to rest in the TA and extensor digitorum, indicating that both muscles were activated during the exercise (figure 3A). For the low b-values (0-100 s mm^{-2}), the signal decayed faster post-exercise compared to pre-exercise, as depicted for the TA in figure 3B. This is reflected in an increased blood flow (F_p×D*) in the TA and extensor digitorum

post-exercise (figure 3C). Combining all volunteers, pre-exercise values in the whole TA were 2.6% ± 0.5% for F_p, 13.9 ± 2.2 ×10^{-3} mm^2 s^{-1} for D*, 0.36 ± 0.10 × 10^{-3} mm^2 s^{-1} for F_p×D*, and 1.57 ± 0.02 × 10^{-3} mm^2 s^{-1} for D. For the whole TA the values for F_p, D* and F_p×D* increased significantly from rest to the recorded recovery period with 63% ± 37%, 58% ± 37%, and 164% ± 108% , respectively (all p<0.001). Also, the diffusion coefficient D of the TA significantly increased after exercise, with 4.0% ± 1.4% (p < 0.001), respectively. The increase in IVIM measures was most prominent in the first half of the number of acquisitions after exercise and recovered slowly to baseline during the second half (figure 3D).

The average F_p×D* over the whole recovery period after exercise (15 min 36 sec) differed between the most distal and most proximal slice, from 0.77 ± 0.33 × 10^{-3} mm^2s^{-1} distally to 1.12 ± 0.46 × 10^{-3} mm^2s^{-1} proximally (p = 0.034) (table 2, figure 3E). The D was lowest at the muscle belly with 1.62 × 10^{-3} ± 0.04 mm^2s^{-1} and there was no difference between the distal and proximal slice (p = 0.063; table 2, figure 3F). The cross-sectional area of the TA for the 8 slices was 3.7 ± 0.7 cm^2, 4.5 ± 0.8 cm^2, 5.0 ± 0.6 cm^2, 5.3 ± 0.8 cm^2, 5.2 ± 0.9 cm^2, 4.8 ± 0.6 cm^2, 4.1 ± 0.8 cm^2, 2.7 ± 1.0 cm^2 from S1 (distal) to S8 (proximal), respectively.

^{31}P MRS

Rest: To establish the origin of the ^{31}P MR signals received by the array coil we analyzed ^{31}P MR images overlaid on anatomical ^{1}H MR images. The ^{31}P signal (being mainly PCr) came for 58% ± 3% (mean ± SEM), 75% ± 3%, 79% ± 3%, 78% ± 2%, and 66% ± 3% from the TA for element E1 to E5, respectively, confirming that the dominant proportion of the ^{31}P signal originated from the TA. The cross-sectional area of the TA at the position of E1 (distal) to E5 (proximal) was 2.6 ± 0.8 cm^2, 4.7 ± 0.8 cm^2, 5.9 ± 0.9 cm^2, 5.2 ± 0.9 cm^2, 2.5 ± 0.9 cm^2, respectively. The summed ^{31}P signal intensity from PCr+Pi+ATP did not differ (p=0.550) between the distal (438 ± 81 × 10^3 a.u) and proximal element (462 ± 80 × 10^3 a.u) of the array coil. However, the phosphorylation potential, as reflected in the PCr/Pi ratio, was significantly lower in the distal element compared to the proximal element (7.0 ± 0.7 vs. 8.9 ± 0.9, p<0.001, table 2).

Continuous isometric exercise: For all five elements, the ^{31}P spectra showed the expected drop in PCr signal and increase in Pi signal during exercise, with post-exercise signal recovery of both, while the three resonances of ATP remained stable (figure 4A/B for E1/E3/E5). In the example illustrated, PCr recovered faster in the proximal element (E5) compared to the distal element (E1). Combining all subjects and coil elements, the average PCr depletion was 48% ± 4%, pH_{endex} was 6.78 ± 0.09, and k_{PCr} was 0.73 ± 0.21 min^{-1}.

The assessment of intramuscular difference along the TA revealed that PCr depletion at the end of exercise was largest for the middle element E3 (54% ± 5%), but not different between the distal and proximal element (p = 0.269) (table 2, figure 5A). The corresponding pH at the end of exercise (pH_{endex}) was higher distally than proximally (6.87 ± 0.10 *vs.* 6.75 ± 0.12, p = 0.033) (table 2, figure 5B). To determine this pH_{endex}, Pi was fitted as two peaks in 47% of all ^{31}P spectra (22% of all distal *vs.* 56% of all proximal spectra) and pH was determined as their average. After exercise, the pH continued to drop for 30 sec in all five elements after which it slowly restored, these temporal pH changes did not differ between the five elements. After exercise, PCr recovered slower (i.e. the rate constant was smaller) for the distal element compared to the proximal element (0.44 ± 0.26 *vs.* 1.50 ± 0.57 min^{-1}; $p < 0.001$) (table 2, figure 5C). The PCr resynthesis, V_{PCr}, was lower distally compared to proximally (5.2 ± 3.1 *vs.* 23.3 ± 8.9 mM min^{-1}; $p < 0.001$) (table 2, figure 5D). To ensure that the fitted k_{PCr} was not corrupted by any movement of the coil, we performed consistency checks. First, we determined the sum of PCr and Pi from spectra obtained during the first 30 sec post-exercise relative to rest. The normalized PCr+Pi values were 0.90 ± 0.08, 0.86 ± 0.06, 0.90 ± 0.05, 0.92 ± 0.06 and 0.92 ± 0.09 for E1 to E5, respectively, indicating no movement effect. Furthermore, k_{PCr} was fitted with the first, the first 4 and the first 8 data points removed. In all cases k_{PCr} still displayed a proximo-distal gradient similar as shown in figure 5C, also indicating that no coil displacement occurred in the early phase of the recovery.

Intermittent isometric exercise: Averaged over the whole TA, intermittent isometric exercise caused a PCr depletion of 44% ± 3%, a pH_{endex} of 6.69 ± 0.20, and a k_{PCr} of 0.95 ± 0.59 min^{-1}. The ^{31}P MR spectra of the five coil elements showed that PCr depletion was, at 49% ± 4%, largest in element 2 (E2), but not different for the distal compared to proximal element (44% ± 3% *vs.* 38% ± 3%, p = 0.068) (table 2, figure 5A). No significant difference in pH_{endex} was observed between the distal and proximal element (6.64 ± 0.21 vs 6.81 ± 0.20, p = 0.138) (table 2, figure 5B). This pH_{endex} was determined as the average of two Pi peaks in 60% of all ^{31}P spectra (80% of all distal *vs.* 40% of all proximal spectra); in the other 40% of the spectra pH_{endex} was determined from a single Pi peak. In line with the recovery after continuous exercise, both k_{PCr} and V_{PCr} were lower distally compared to proximally for the intermittent exercise (0.70 ± 0.65 *vs.* 1.66 ± 1.00 min^{-1}; p = 0.043 and 8.7 ± 8.1 *vs.* 22.2 ± 14.2 mM min^{-1}; p = 0.043, respectively) (table 2, figure 5E/F).

Carnosine

In ^{1}H MR spectra of all 6 volunteers carnosine signals were visible in the distal and proximal voxel at 7 and 8 ppm (figure 6). The signal integral of the 8 ppm carnosine peak relative to the water signal at rest did not differ between the distal and the proximal voxel ($1.74 \times 10^{-6} \pm 0.42 \times 10^{-6}$ *vs.* $1.71 \times 10^{-6} \pm 0.48 \times 10^{-6}$, $p = 0.884$, table 2).

Statistical outcomes of mixed model and correlation analysis

The outcomes of the statistical analysis with mixed models for the NIRS, IVIM and ^{31}P MRS measurements during and following continuous isometric exercise are presented in table 3. For the NIRS, the relation between k_{O2Hb} and the 7 locations along the TA was best fitted with a linear mixed model, whereby optode location had a significant effect on k_{O2Hb} ($p < 0.001$).

The IVIM parameters $F_p \times D^*$ and D were best fitted with a non-linear model, with p-values for location^2 being $p = 0.003$ and $p < 0.001$, respectively. For location we obtained $p = 0.087$ and $p < 0.001$, respectively.

For the ^{31}P MRS results of the TA at rest the PCr/Pi ratio was linearly related to the coil element number (location: $p < 0.001$). The post-exercise variables, k_{PCr} and V_{PCr} showed a significant non-linear relationship with coil element number for the continuous isometric exercise (location: $p = 0.060$ and $p = 0.444$, location^2: $p = 0.001$ and $p = 0.028$, respectively), which in case of k_{PCr} could not be explained by the covariate pH_{endex} ($p = 0.207$). Furthermore, pH_{endex} and PCr depletion showed a significant non-linear association with coil element number (location: $p = 0.002$ and $p < 0.001$, and location^2: $p = 0.008$ and $p < 0.001$, respectively).

For the intermittent isometric exercise, the mixed model did not converge, presumably due to the lack of power with only 5 subjects. Nevertheless, it did show a trend that k_{PCr}, PCr depletion and V_{PCr} correlated with location, consistent with the results of the continuous isometric exercise.

The correlation analysis revealed that k_{PCr} correlated strongly with k_{O2Hb} ($r = 0.956$, $p = 0.011$) and $F_p \times D^*$ ($r = 0.932$, $p = 0.021$) (figure 7A/B). The PCr resynthesis rate V_{PCr} also strongly correlated with $F_p \times D^*$ ($r = 0.985$, $p = 0.002$) and showed a trend in the correlation with k_{O2Hb} ($r = 0.852$, $p = 0.067$) (figure C/D).

Discussion

In this study we investigated spatially specific interactions between O_2 supply and consumption, and the generation of biochemical free energy (ATP, PCr) along the length of the working human tibialis anterior. To examine this physiology *in vivo* we combined spatially resolved data measured by NIRS for O_2Hb, MRI (IVIM) for perfusion and ^{31}P MRS for energy metabolism before, during and after isometric exercise of this muscle.

We observed that following continuous isometric ankle dorsiflexion at 30% maximum force until exhaustion, the recovery rate constants of O_2Hb (k_{O2Hb}) and of PCr (k_{PCr}), as well as perfusion (F_pxD*), and the absolute rate of PCr recovery (k_{PCr}×ΔPCr) increased from distal to proximal along the length of the TA. As PCr resynthesis is proportional to the oxygen dependent suprabasal ATP synthesis, and as additionally O_2Hb recovers faster proximally than distally this indicates that O_2 supply also exhibits a proximo-distal gradient with the highest O_2 supply proximally. Furthermore, we found that following intermittent isometric exercise k_{PCr} also increased from distal to proximal along the TA, indicating that prolonged ischemia during exercise cannot explain the observed gradient in k_{PCr} and O_2 supply following exercise. In contrast to these proximo-distal gradients occurring upon exercise the relative carnosine content did not differ between the distal and proximal part of the TA, indicating no major variation in fiber type.

The recovery rate constant k_{PCr} is a well-established marker of muscle mitochondrial function, reflecting maximal potential capacity for oxidative ATP synthesis (Q_{max}). The Q_{max} derived from our ^{31}P data showed a similar proximo-distal gradient (data not shown). However, Q_{max} is a function based on severable variables and assumptions, wherefore we chose to focus on k_{PCr} instead, because it is simpler and more robust than Q_{max}. When O_2 supply is not limiting, k_{PCr} correlates with biopsy measures of mitochondrial content and function (Kemp *et al.*, 2015). Studies typically compare k_{PCr} before and after an intervention, and/or between a disease and control group. In those studies, faster PCr recovery kinetics, indicative of greater 'mitochondrial function', represent better muscle performance. It is interesting to compare the spatially dependent k_{PCr} values in our study to those determined without an attempt to define the measurement location along the TA. In 8 such studies reviewed in (Kemp *et al.*, 2015), the mean value is 1.35 min^{-1}, which is closer to the proximal than the distal k_{PCr} values in the present study (see table 2).

Intramuscular differences in k_{PCr} have also been observed in the gastrocnemius muscle (Niess *et al.*, 2020). In contrast to our study PCr recovery after exercise was faster distally than proximally and the difference was much smaller (1.25 min^{-1} vs. 1.00 min^{-1}) than in the TA (0.44 min^{-1} vs. 1.50 min^{-1}). These two studies are difficult to compare, because the 8 cm distal-proximal length studied in the gastrocnemius medialis corresponds to a coverage of only two of our adjacent ^{31}P coil elements. Our results show that differences between two elements highly depends on where they are located along the muscle (see figure 5).

With the present study, applying continuous isometric ankle dorsiflexion at 30% MVC until exhaustion, we confirm our earlier observation of a substantial negative proximo-distal gradient in k_{PCr} along the TA after ankle dorsiflexion, but performed at 60% MVC for 40 sec (Boss *et al.*, 2018). Moreover, this gradient in the TA was also observed after incremental exercise at several intensities until exhaustion and after intermittent isometric exercise.

The type of exercise might influence the spatial k_{PCr} gradient in two ways, via spatial variation in the degree of ischemia caused by the isometric exercise and via end-exercise pH. Ischemia is not likely to play a major role, since the proximo-distal gradient in k_{PCr} is essentially the same with intermittent isometric exercise, in which the contraction pattern has less scope for interfering with blood flow. Cytosolic acidification, measured by end-exercise pH, has a complex effect on PCr recovery, tending to decrease k_{PCr} (Walter *et al.*, 1997; van den Broek *et al.*, 2007; Kemp *et al.*, 2015). In the present study, the TA exhibited significant cytosolic acidification near end-exercise, with the most severe acidification in the proximal part of the TA, where k_{PCr} was highest, clearly ruling out pH as a potential factor. During the intermittent exercise, by contrast, the lowest pH was found in the distal part of the muscle. However, the proximo-distal pH difference of 0.2 is not large enough to explain a two-fold proximo-distal difference in k_{PCr} (Bendahan *et al.*, 1990; van den Broek *et al.*, 2007). In the 40 sec submaximal exercise no pH drop was observed (Boss *et al.*, 2018). In none of the cases does end-exercise pH emerge as a significant factor in the mixed model analysis. Therefore, we can conclude that proximo-distal variation in pH does not explain the proximo-distal gradient in k_{PCr}.

Is it possible that the spatial variation in k_{PCr} depends on a proximo-distal gradient in O_2 supply? The muscle has relatively little O_2 storage capacity so the rates of net O_2 supply and O_2 usage are closely coupled. Net O_2 consumption is the product of the arterial venous oxygen difference (AVD) and blood flow, thus for any rate of O_2 use the O_2 supply can be matched by appropriate changes in AVD or blood flow. Changes in AVD could in theory be assessed via

amplitude changes in the NIRS deoxyhemoglobin signal. However, these amplitude changes are highly dependent on the ratio between the active tissue volume and assessed tissue volume. This ratio is unknown and likely to vary along the TA, and therefore the change in AVD cannot be reliable assessed. We therefore have no direct evidence on AVD, but in the absence of large changes in AVD we would therefore expect absolute blood flow to track O_2 supply and thus O_2 consumption, spatially.

There has been much interest in proximo-distal gradients in muscle blood flow and O_2 supply and O_2 use. Generally speaking these studies are in line with the proximo-distal gradients we found in k_{O2Hb} and muscle perfusion (F_pxD*), both being lower in the distal part of the TA, suggesting lower O_2 supply in distal compared to proximal muscle (Miura *et al.*, 2001; Mizuno *et al.*, 2003; Crenshaw *et al.*, 2010; Niess *et al.*, 2020). This is reflected in larger NIRS changes (deoxygenation) in the distal part of the vastus lateralis and gastrocnemius (Miura *et al.*, 2001; Crenshaw *et al.*, 2010). Furthermore, an MRI study using arterial spin label (ASL) showed a lower muscle perfusion more distally in the gastrocnemius (Niess *et al.*, 2020). Direct comparison of these studies with our work are problematic as we investigated spatial variations along nearly the whole TA, covering 20 cm, while the coverage of the NIRS and ASL studies was 10 cm and 8 cm, respectively. Furthermore, for NIRS, these studies reported absolute recovery rates, while we assessed recovery rate constants. In a study using positron emission tomography ($H_2^{15}O$ PET), both blood flow and O_2 uptake increased from distal to proximal in the quadriceps muscles during rest, but this gradient disappeared following exhaustive exercise (Mizuno *et al.*, 2003). There appear to be no previous studies of this phenomenon in human TA, but, agreeing with our study, the TA in the rat has a higher capillary density proximally compared to distally (Torrella *et al.*, 2000).

There is no doubt that mitochondrial function as measured by ^{31}P MRS and muscle blood flow are related. For example, there is a correlation between whole muscle k_{PCr} and post-exercise perfusion determined by ASL (Duteil *et al.*, 2004; Carlier *et al.*, 2006). Furthermore, while whole muscle k_{PCr} in untrained subjects does not increase with an increase in the fraction of inspired oxygen, suggesting that O_2 supply is normally not a limiting factor for PCr recovery, it does decrease when the fraction of inspired oxygen is decreased (Haseler *et al.*, 2004, 2007).

If the primary cause of slower PCr recovery distally is a lower perfusion, limiting oxidative ATP synthesis, then we expect an increased average rate and extent of both deoxygenation and PCr fall during exercise (assuming no significant spatial gradients in ATP demand), followed post-

exercise by decreased rate constants of both PCr resynthesis and reoxygenation, in distal compared to proximal muscle (Kemp *et al.*, 1995, 2001). According to the equation V_{PCr} = k_{PCr}×ΔPCr, given exponential recovery kinetics, a lower PCr resynthesis rate after the same or a greater fall in PCr amounts to a decreased PCr recovery rate constant (ratio of the two quantities (k_{PCr} = V_{PCr}/ΔPCr). We do in fact observe a decreased V_{PCr} and k_{PCr} distally, but no difference in ΔPCr. By an analogous argument, a lower reoxygenation rate from the same or a lower state of oxygenation amounts to a decreased reoxygenation recovery rate constant (k_{O2Hb}). We do see a decreased k_{O2Hb} in distal muscle. Across the spatial gradient, the rate constants k_{PCr} and k_{O2Hb} would change in the same direction, as we indeed observed. However, if the primary cause was vascular the relative 'abnormality' (i.e. in distal relative to proximal) in reoxygenation would exceed that in PCr recovery: a pattern seen in e.g. moderate peripheral vascular disease (Kemp *et al.*, 2001). But this is not what we see in TA, where the differences in PCr recovery kinetics are proportionally twice as great as the reoxygenation kinetics. This makes it highly unlikely that lower perfusion in the distal part of the muscle explains the spatial variation in k_{PCr}.

Consider now the alternate situation that the spatial variations in k_{PCr}, k_{O2Hb} and IVIM perfusion measures all are determined by a lower intrinsic mitochondrial function distally. In general, in the face of impaired mitochondrial function, oxidative ATP synthesis rate can be maintained to some extent by classical closed-loop feedback (increased fall in PCr, rise in [ADP], etc) (Kemp *et al.*, 2015). A lower mitochondrial function distally, up to a certain energy demand, V_{PCr} can thus be maintained at the expense of a bigger ΔPCr, implying a lower k_{PCr} (k_{PCr} =V_{PCr}/ΔPCr); beyond that energy demand V_{PCr} cannot be maintained and then k_{PCr} is even lower. What are the implications for NIRS kinetics? A lower distal V_{PCr} implies that O_2 use is lower distally. If O_2 supply is matched to O_2 use, deoxygenation will be less distally and one might expect k_{O2Hb} therefore to be higher distally. In fact we observe that k_{O2Hb} is slightly lower distally. However, it can be questioned if O_2 supply and O_2 use are exactly matched, since the NIRS recovery kinetics are dominated by O_2 delivery rather than use of O_2 (as post-exercise O_2 supply drives oxygenation state back to baseline). This makes it difficult to predict how k_{O2Hb} will behave in the situation of spatial variation of mitochondrial function. A higher intrinsic mitochondrial function proximally could be due to a higher mitochondrial content proximally (Park *et al.*, 2014), but there is no existing data on the distribution of mitochondrial content along the human TA.

Note that lower intrinsic mitochondrial capacity might also explain the lower resting phosphorylation potential (PCr/Pi) observed distally. This increased distal feedback signal is necessary to maintain resting ATP synthesis rate despite a spatial variation in mitochondrial function operating across the whole dynamic range of muscle power (Kemp *et al.*, 2015). Instead it is hard to explain lower resting phosphorylation potential in terms of reduced vascular O_2 supply distally, which is not expected to be limiting at rest.

The similar PCr and pH decline proximally and distally during exercise, in particular during submaximal exercise (Boss et al, 2018), suggests that energy expenditure at both ends of the TA is not much different. So the question is what functional differences between proximal and distal parts of the TA are served by higher proximal rates of PCr recovery, perfusion and oxygenation after exercise? Proximally the TA arises from the lateral condyle and upper lateral surface of the tibia and converges into a belly shaped fleshy muscle with a relatively large cross-sectional area, while distally this area becomes smaller and at about 1/3 of the tibia the TA is linked to a tendon. So this anatomical variance suggests that a more proximally higher contractile property is associated with faster post-exercise energy recovery. Is this reflected in a proximo-distal variation in fiber type distribution, organization or properties? It has been reported that the human TA consists of about 70% oxidative fibers, but to our knowledge there are no studies on fiber type distribution along the length of the TA in humans (Johnson *et al.*, 1973). Our observation that tissue levels of carnosine, as surrogate fiber type marker (C. Harris *et al.*, 1998), are similar along the TA suggests that a proximo-distal variation in fiber type is not important, though this needs to be confirmed by more direct measurements. Studies in rats and rabbits found that the area occupied by oxidative fibers in TA increases from distal to proximal, indicating increased mitochondrial capacity (Wang and Kernell, 2001). The human TA has a bipennate fiber architecture in which the axial orientation of the aponeurosis varies along the length of the muscle and the pennation angle increases in the distal-proximal direction from 7° to 15° (Hiblar *et al.*, 2003; Lansdown *et al.*, 2007), although an earlier study reported no such variation in pennation angle (Maganaris and Baltzopoulos, 1999). Sarcomeres in fibers of the rat TA have different lengths between the distal and proximal parts of this muscle, of which the size depends on knee angle (Tijs *et al.*, 2015). It has also been demonstrated that the TA may contain hybrid fibers with different myosin heavy chain expression (Medler, 2019). These different contractile structures may have different post-exercise requirements for energy recovery. Finally, it may be argued that the lower distal k_{PCr} is due to more connective and fibrous tissue. However, these tissues do not contribute to

568 the PCr signal involved in the k_{PCr} assessment and we observed that the (PCr + Pi + ATP) signal
569 intensity is similar between the proximal and distal parts of the TA covered by the ^{31}P array
570 coil, indicating similar muscle content in these parts.

571 Whatever the underlying physiology, our work also has several methodological implications.
572 The magnitude of the differences in k_{O2Hb}, $F_p \times D^*$,and k_{PCr} that we observed along the TA is
573 comparable to differences in these variables observed in muscle diseases vs. healthy controls
574 or the effect of training measured at a single muscle location. For instance, variations in k_{O2Hb}
575 are in the order of the difference between healthy subjects and patients with chronic heart
576 failure and peripheral vascular disease (McCully *et al.*, 1997; Hanada *et al.*, 2000), in $F_p \times D^*$ the
577 variations are as between the soleus and the gastrocnemius muscle (Mastropietro *et al.*,
578 2018), and for k_{PCr}, the differences are as between untrained and endurance-trained TA
579 (Larsen *et al.*, 2009). This highlights the critical selection of a suitable measurement location
580 and assuring reproducible repositioning in follow-up studies for O_2 supply and energy
581 metabolic measurements, as a single location within the muscle might not represent the
582 muscle as a whole. Furthermore, the significant variation in k_{O2Hb} and F_pxD* along the length of
583 TA is in line with our previous muscle functional MRI (mf-MRI) findings revealing a proximo-
584 distal gradient in the slope of the mf-MRI signal increase after exercise (Boss *et al.*, 2018).
585 However, the mf-MRI signal recovers 2-3 times slower than the NIRS O_2Hb signal, suggesting
586 that mf-MRI reflects not only changes in oxygenation, but most likely also changes in T2
587 relaxation time due to other factors, like intra- and extracellular water shifts (Meyer and Prior,
588 2000; Damon and Gore, 2005; Schmid *et al.*, 2014).

589 The present study was limited to young male subjects, in whom a thin subcutaneous fat layer
590 facilitated a good SNR of the ^{31}P MR and NIRS spectra in the TA. Future studies on whether this
591 observed proximo-distal gradient changes with age or training, and differs between women
592 and men, could give additional information on underlying mechanisms and muscle function. It
593 is also of interest to assess if the intramuscular variation in k_{PCr} occurs in other muscles such as
594 the gastrocnemius and vastus lateralis, for which intramuscular variation in oxygenation and
595 blood flow was already demonstrated. Mapping such intramuscular differences in multiple
596 muscles could help to understand pathophysiological mechanisms in muscle disorders. For
597 example, in muscular dystrophy patients, it is unknown yet why the disease spreads non-
598 uniformly along the proximo-distal axis (Janssen *et al.*, 2014; Hooijmans *et al.*, 2017).

In conclusion, we provide evidence that in the human tibialis anterior the post-exercise O_2 supply is higher proximal than distal, which is associated with a higher proximal PCr recovery rate constant k_{PCr} and resynthesis rate V_{PCr}. Our experimental findings suggest that a higher intrinsic mitochondrial capacity could be the major factor underlying this proximal higher O_2 supply and PCr recovery, apparently to serve a quick recovery of energy in the main contractile element of this muscle.

References

Arnold DL, Taylor DJ, Radda GK. Investigation of human mitochondrial myopathies by phosphorus magnetic resonance spectroscopy. Ann. Neurol. 1985; 18: 189–196.

Baguet A, Everaert I, Hespel P, Petrovic M, Achten E, Derave W. A new method for non-invasive estimation of human muscle fiber type composition. PLoS One 2011; 6: e21956.

Bendahan D, Confort-Gouny S, Kozak-Reiss G, Cozzone PJ. Heterogeneity of metabolic response to muscular exercise in humans. New criteria of invariance defined by in vivo phosphorus-31 NMR spectroscopy. FEBS Lett. 1990; 272: 155–8.

Le Bihan D, Breton E, Lallemand D, Aubin ML, Vignaud J, Laval-Jeantet M. Separation of diffusion and perfusion in intravoxel incoherent motion MR imaging. Radiology 1988; 168: 497–505.

Boss A, Heskamp L, Breukels V, Bains LJ, van Uden MJ, Heerschap A. Oxidative capacity varies along the length of healthy human tibialis anterior. J. Physiol. 2018; 596: 1467–1483.

van den Broek NMA, Graaf L De, Nicolay K, Prompers JJ. Intersubject differences in the effect of acidosis on phosphocreatine recovery kinetics in muscle after exercise are due to differences in proton efflux rates. Am. J. Physiol. - Cell Physiol. 2007; 293: 228–237.

C. Harris R, Dunnett M, Greenhaff PL. Carnosine and taurine contents in individual fibres of human vastus lateralis muscle. J. Sports Sci. 1998; 16: 639–643.

Carlier PG, Bertoldi D, Baligand C, Wary C, Fromes Y. Muscle blood flow and oxygenation measured by NMR imaging and spectroscopy. NMR Biomed. 2006; 19: 954–67.

Craig CL, Marshall AL, Sjöström M, Bauman AE, Booth ML, Ainsworth BE, et al. International physical activity questionnaire: 12-Country reliability and validity. Med. Sci. Sports Exerc. 2003; 35: 1381–1395.

Crenshaw AG, Bronee L, Krag I, Jensen BR. Oxygenation and EMG in the proximal and distal vastus lateralis during submaximal isometric knee extension. J. Sports Sci. 2010; 28: 1057–1064.

Damon BM, Gore JC. Physiological basis of muscle functional MRI: predictions using a computer model. J Appl Physiol 2005; 98: 264–273.

633 Duteil S, Bourrilhon C, Raynaud JS, Wary C, Richardson RS, Leroy-Willig A, et al. Metabolic and
634 vascular support for the role of myoglobin in humans: a multiparametric NMR study. Am. J.
635 Physiol. Integr. Comp. Physiol. 2004; 287: R1441–R1449.

636 Ferrari M, Wei Q, Carraresi L, De Blasi RA, Zaccanti G. Time-resolved spectroscopy of the
637 human forearm. J. Photochem. Photobiol. B. 1992; 16: 141–53.

638 Fleischman A, Makimura H, Stanley TL, McCarthy MA, Kron M, Sun N, et al. Skeletal muscle
639 phosphocreatine recovery after submaximal exercise in children and young and middle-aged
640 adults. J. Clin. Endocrinol. Metab. 2010; 95: E69-74.

641 Hanada A, Okita K, Yonezawa K, Ohtsubo M, Kohya T, Murakami T, et al. Dissociation between
642 muscle metabolism and oxygen kinetics during recovery from exercise in patients with chronic
643 heart failure. Heart 2000; 83: 161–6.

644 Harris RC, Edwards RHT, Hultman E, Nordesjö LO, Nylind B, Sahlin K. The time course of
645 phosphorylcreatine resynthesis during recovery of the quadriceps muscle in man. Pflügers
646 Arch. Eur. J. Physiol. 1976; 367: 137–142.

647 Haseler LJ, Lin A, Hoff J, Richardson RS. Oxygen availability and PCr recovery rate in untrained
648 human calf muscle: evidence of metabolic limitation in normoxia. Am. J. Physiol. Regul. Integr.
649 Comp. Physiol. 2007; 293: R2046-51.

650 Haseler LJ, Lin AP, Richardson RS. Skeletal muscle oxidative metabolism in sedentary humans:
651 31P-MRS assessment of O2 supply and demand limitations. J. Appl. Physiol. 2004; 97: 1077–81.

652 Hiblar T, Bolson EL, Hubka M, Sheehan FH, Kushmerick MJ. Three dimensional ultrasound
653 analysis of fascicle orientation in human tibialis anterior muscle enables analysis of
654 macroscopic torque at the cellular level. Adv. Exp. Med. Biol. 2003

655 Hooijmans MT, Niks EH, Burakiewicz J, Anastasopoulos C, van den Berg SI, van Zwet E, et al.
656 Non-uniform muscle fat replacement along the proximodistal axis in Duchenne muscular
657 dystrophy. Neuromuscul. Disord. 2017; 27: 458–464.

658 Janssen BH, Voet NBM, Nabuurs CI, Kan HE, De Rooy JWJ, Geurts AC, et al. Distinct disease
659 phases in muscles of facioscapulohumeral dystrophy patients identified by MR detected fat
660 infiltration. PLoS One 2014; 9: e85416.

661 Johnson MA, Polgar J, Appleton D. Data on the Distribution of Fibre Types in Thirty-six Human
662 Muscles An Autopsy Study. J Neurol Sci 1973; 18: 111–29.

663 Kemp GJ, Ahmad RE, Nicolay K, Prompers JJ. Quantification of skeletal muscle mitochondrial
664 function by 31P magnetic resonance spectroscopy techniques: a quantitative review. Acta
665 Physiol. (Oxf). 2015; 213: 107–144.

666 Kemp GJ, Roberts N, Bimson WE, Bakran A, Harris PL, Gilling-Smith GL, et al. Mitochondrial
667 function and oxygen supply in normal and in chronically ischemic muscle: A combined 31P
668 magnetic resonance spectroscopy and near infrared spectroscopy study in vivo. J. Vasc. Surg.
669 2001; 34: 1103–1110.

670 Kushmerick M. J., Meyer RA, Brown TR. Regulation of oxygen consumption in fast- and slow-
671 twitch muscle. Am. J. Physiol. Physiol. 1992; 263: C598–C606.

672 Kushmerick Martin J., Moerland TS, Wiseman RW. Mammalian skeletal muscle fibers
673 distinguished by contents of phosphocreatine, ATP, and Pi. Proc. Natl. Acad. Sci. 1992; 89:
674 7521–7525.

675 Lansdown DA, Ding Z, Wadington M, Hornberger JL, Damon BM. Quantitative diffusion tensor
676 MRI-based fiber tracking of human skeletal muscle. J. Appl. Physiol. 2007; 103: 673–81.

677 Larsen RG, Callahan DM, Foulis SA, Kent-Braun JA. In vivo oxidative capacity varies with muscle
678 and training status in young adults. J. Appl. Physiol. 2009; 107: 873–879.

679 Maganaris CN, Baltzopoulos V. Predictability of in vivo changes in pennation angle of human
680 tibialis anterior muscle from rest to maximum isometric dorsiflexion. Eur. J. Appl. Physiol.
681 Occup. Physiol. 1999; 79: 294–7.

682 Mastropietro A, Porcelli S, Cadioli M, Rasica L, Scalco E, Gerevini S, et al. Triggered intravoxel
683 incoherent motion MRI for the assessment of calf muscle perfusion during isometric
684 intermittent exercise. NMR Biomed. 2018; 31: 1–13.

685 McCully KK, Fielding RA, Evans WJ, Leigh JS, Posner JD. Relationships between in vivo and in
686 vitro measurements of metabolism in young and old human calf muscles. J. Appl. Physiol.
687 1993; 75: 813–819.

688 McCully KK, Hamaoka T. Near-infrared spectroscopy: what can it tell us about oxygen

689 saturation in skeletal muscle? Exerc. Sport Sci. Rev. 2000; 28: 123–7.

690 McCully KK, Landsberg L, Suarez M, Hofmann M, Posner JD. Identification of peripheral
691 vascular disease in elderly subjects using optical spectroscopy. J. Gerontol. A. Biol. Sci. Med.
692 Sci. 1997; 52: B159-65.

693 Medler S. Mixing it up: the biological significance of hybrid skeletal muscle fibers. J. Exp. Biol.
694 2019; 222: jeb200832.

695 Meyer A. A linear model of muscle respiration explains monoexponential phosphocreatine
696 changes. Am. J. Physiol. 1988; 254: C548–C553.

697 Meyer RA, Brown TR, Kushmerick MJ. Phosphorus nuclear magnetic resonance of fast- and
698 slow-twitch muscle. Am. J. Physiol. Physiol. 1985; 248: C279–C287.

699 Meyer RA, Prior BM. Functional magnetic resonance imaging of muscle. Exerc Sport Sci Rev
700 2000; 28: 89–92.

701 Miura H, McCully K, Hong L, Nioka S, Chance B. Regional difference of muscle oxygen
702 saturation and blood volume during exercise determined by near infrared imaging device. Jpn.
703 J. Physiol. 2001; 51: 599–606.

704 Mizuno M, Mimura Y, Iwakawa T, Oda K, Ishii K, Ishiwata K, et al. Regional differences in blood
705 flow and oxygen consumption in resting muscle and their relationship during recovery from
706 exhaustive exercise. J. Appl. Physiol. 2003; 95: 2204–2210.

707 Moon RB, Richards JH. Determination of intracellular pH by 31P magnetic resonance. J. Biol.
708 Chem. 1973; 248: 7276–7278.

709 Naressi A, Couturier C, Devos JM, Janssen M, Mangeat C, Beer R de, et al. Java-based graphical
710 user interface for the MRUI quantitation package. Magma Magn. Reson. Mater. Physics, Biol.
711 Med. 2001; 12: 141–152.

712 Niess F, Schmid AI, Bogner W, Wolzt M, Carlier P, Trattnig S, et al. Interleaved 31 P MRS/ 1 H
713 ASL for analysis of metabolic and functional heterogeneity along human lower leg muscles at
714 7T. Magn. Reson. Med. 2020; 83: 1909–1919.

715 Park S-Y, Gifford JR, Andtbacka RHI, Trinity JD, Hyngstrom JR, Garten RS, et al. Cardiac, skeletal,
716 and smooth muscle mitochondrial respiration: are all mitochondria created equal? [Internet].

717 Am. J. Physiol. Heart Circ. Physiol. 2014; 307: H346-52.Available from:
718 http://www.ncbi.nlm.nih.gov/pubmed/24906913

719 Phielix E, Schrauwen-Hinderling VB, Mensink M, Lenaers E, Meex R, Hoeks J, et al. Lower
720 intrinsic ADP-stimulated mitochondrial respiration underlies in vivo mitochondrial dysfunction
721 in muscle of male type 2 diabetic patients. Diabetes 2008; 57: 2943–2949.

722 Schiaffino S, Reggiani C. Fiber Types in Mammalian Skeletal Muscles. Physiol. Rev. 2011; 91:
723 1447–1531.

724 Schmid AI, Schewzow K, Fiedler GB, Goluch S, Laistler E, Wolzt M, et al. Exercising calf muscle
725 T2 * changes correlate with pH, PCr recovery and maximum oxidative phosphorylation. NMR
726 Biomed 2014; 27: 553–60.

727 Söderlund K, Hultman E. ATP and phosphocreatine changes in single human muscle fibers after
728 intense electrical stimulation. Am. J. Physiol. 1991; 261: E737–E741.

729 Stefan D, Cesare F Di, Andrasescu A, Popa E, Lazariev A, Vescovo E, et al. Quantitation of
730 magnetic resonance spectroscopy signals : the jMRUI software package. Meas. Sci. Technol
731 2009; 20: 1–9.

732 Takahashi H, Kuno S, Katsuta S, Shimojo H, Masuda K, Yoshioka H, et al. Relationships between
733 Fiber Composition and NMR Measurements in Human Skeletal Muscle. NMR Biomed. 1996; 9:
734 8–12.

735 Taylor DJ, Bore PJ, Styles P, Gadian DG, Radda GK. Bioenergetics of intact human muscle. A 31P
736 nuclear magnetic resonance study. Mol Biol Med 1983; 1: 77–94.

737 Tijs C, van Dieën JH, Maas H. Effects of epimuscular myofascial force transmission on
738 sarcomere length of passive muscles in the rat hindlimb. Physiol. Rep. 2015; 3

739 Torrella JR, Whitmore JM, Casas M, Fouces V, Viscor G. Capillarity, fibre types and fibre
740 morphometry in different sampling sites across and along the tibialis anterior muscle of the
741 rat. Cells. Tissues. Organs 2000; 167: 153–162.

742 van Uden MJ, Veltien A, Janssen BH, Heerschap A. 1H/31P birdcage coil combined with
743 dedicated multi-element 31P receive coil for optimal 31P MRSI of the tibialis anterior . Proc.
744 Intl. Soc. Mag. Reson. Med. 2012; 20

745 Walter G, Vandenborne K, McCully KK, Leigh JS. Noninvasive measurement of phosphocreatine
746 recovery kinetics in single human muscles. Am. J. Physiol. 1997; 272: C525-34.

747 Wang LC, Kernell D. Fibre type regionalisation in lower hindlimb muscles of rabbit, rat and
748 mouse: a comparative study. J. Anat. 2001; 199: 631–43.

749 Yoshida T, Abe D, Fukuoka Y. Phosphocreatine resynthesis during recovery in different muscles
750 of the exercising leg by 31P-MRS. Scand J Med Sci Sport. 2013; 23: e313-9.

751

Additional information

Data availability statement

The data that support the findings of this study are available from the corresponding author upon reasonable request.

Competing interests

All authors have nothing to declare.

Author contribution

The experiments where performed at the department of Medical Imaging/Radiology of the Radboud university medical center, Nijmegen, The Netherlands. L.H, A.B, and A.H. were involved in the conception or design of the work. M.J.U built the ^{31}P-coil and helped to develop the experimental set-up. L.H. and F.B were involved in the acquisition and analysis of the data and drafting the work. M.F provided help with the sequence optimization and analysis of the IVIM data. M.M was involved in optimizing the IVIM sequence and in the statistical analysis. J.C contributed to the NIRS data-acquisition and analysis. L.H, F.L, G.K, A.B, and A.H contributed to the interpretation of the work. All authors were involved in revising the work critically for important intellectual content.

All authors approved the final document and agreed to be accountable for all aspects of the work in ensuring that questions related to the accuracy or integrity of any part of the work are appropriately investigated and resolved. All persons designated as authors qualify for authorship, and all those who qualify for authorship are listed.

Funding

L.H was supported by the European Community's Seventh Framework Programme (FP7/2007–2013) under grant agreement number 305697. A.B was supported by fundings from the Centre for Systems Biology and Bioenergetics, Radboud University Nijmegen, the Netherlands.

Acknowledgements

We would like to thank the volunteers for their dedication to the study and Dr. Huub Maas for valuable comments.

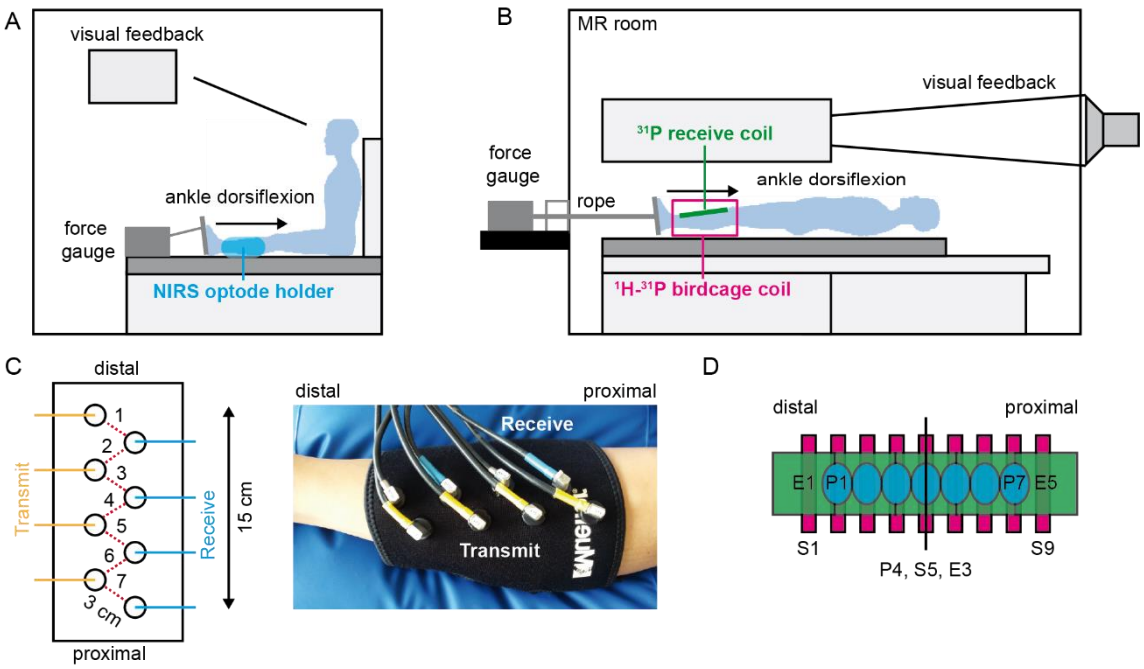

Figure 1: Schematic overview of the experimental approach. A) Set-up for the NIRS measurement. The subject's foot was placed in a shoe attached to a pedal connected to a force gauge. The place of the NIRS optode holder is indicated in blue. B) Set-up for the MRI measurements. The subject's foot was placed in a shoe attached to a pedal and connected with a rope to a force gauge outside the scanner room. The subject received visual feedback by a beamer placed in the controller room. C) Overview of the placement of the four transmit and four receive optodes (all 3 cm apart) for the NIRS measurement, allowing oxyhemoglobin assessment at seven positions along the muscle. D) Schematic overview of the positioning of the seven NIRS measurement locations (blue, P1 to P7), the nine diffusion weighted slices (pink, S1 to S9) and the five ^{31}P coil elements (green, E1 to E5). The middle positions (P4, S5, and E3) were centred at 1/3 the distance between the fibula head and lateral malleolus, near the muscle belly. The 20 cm long ^{31}P array coil covers the voluminous part of the TA.

Table 1: Subject characteristics – demographics and self-reported physical activity for the fifteen volunteers doing continuous isometric exercise

Demographics	
Age (years)	26 ± 3
Weight (kg)	76.1 ± 8.8
Height (m)	1.82 ± 0.08
BMI (kg m^{-2})	22.8 ± 1.5
Self-reported physical activity	
Sitting (h:min per day)	7:18 ± 2:22 (3:51 to 11:09)
Walking (h:min per week)	4:58 ± 4:15 (0:30 to 16:40)
Cycling (h:min per week)	2:46 ± 2:36 (0:00 to 7:00)
Heavy intensity activities (h:min per week)	2:58 ± 2:35 (0:00 to 10:00)
Medium intensity activities (h:min per week)	5:48 ± 9:21 (0:00 to 36:00)

Data are presented as mean ± SD for demographics and mean ± SD (min to max) for self-reported physical activity.

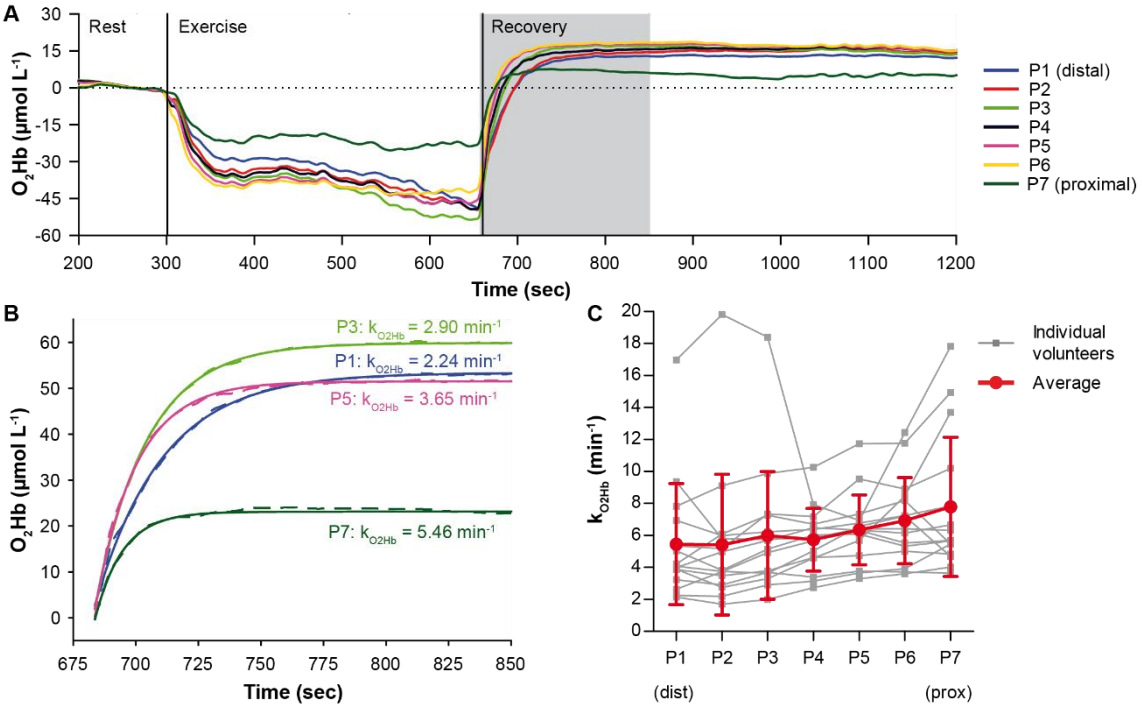

800

801 **Figure 2:** Time and spatial variations in the change in tissue oxyhemoglobin (O_2Hb)
802 concentration assessed with near infrared spectroscopy (NIRS) in exercise experiments. A)
803 Typical example of one volunteer for the change in tissue O_2Hb concentration during rest,
804 exercise and recovery. Data is shown from the last 100 sec of rest to 1200 sec after the start of
805 the experiment. An expansion of the time window during recovery, indicated by the grey
806 block, is in B. B) Recovery of O_2Hb, baseline-corrected to end-exercise values, during the first
807 170 sec after exercise for optode position P1 (distal), P3, P5, and P7 (proximal) depicted as
808 dashed lines. The corresponding mono-exponential fit is depicted as solid lines. C) Recovery
809 rate constant of O_2Hb (k_{O2Hb}) for each volunteer per optode position and averaged over all
810 volunteers (P1 distal, P7 proximal). The linear gradient in k_{O2Hb} was 0.15 $min^{-1}cm^{-1}$ (standard
811 error: 0.04 $min^{-1}cm^{-1}$) Data are presented as mean ± SD.

Table 2: Outcome measures of NIRS, IVIM, ^{31}P MRS and ^{1}H MRS and cross-sectional area along the length of the tibialis anterior muscle.

	n	Distal	Middle	Proximal	p-value distal *vs.* proximal
Group continuous exercise – Subjects 1 to 15					
NIRS					
k_{O2Hb} (min^{-1})	15	5.4 ± 3.8	5.7 ± 2.0	7.8 ± 4.4	0.011
IVIM					
CSA (cm^2)	13	3.7 ± 0.7	5.2 ± 0.9	2.7 ± 1.0	0.025
D (mm^2 s^{-1})	13	1.64 ± 0.04	1.62 ± 0.03	1.66 ± 0.05	0.063
F_p×D* ($x10^{-3}$ mm^2 s^{-1})	13	0.77 ± 0.33	0.84 ± 0.14	1.12 ± 0.46	0.034
^{31}P MRS					
CSA (cm^2)	10	2.6 ± 0.8	5.9 ± 0.9	2.5 ± 0.9	0.712
PCr/Pi in rest	10	7.0 ± 0.7	8.3 ± 1.5	8.9 ± 0.9	p<0.001
PCr depletion (%)	10	41 ± 7	54 ± 5	45 ± 10	0.269
pH_{endex}	9	6.87 ± 0.10	6.74 ± 0.09	6.75 ± 0.12	0.033
pH1 (range; n)		6.88 – 7.07; 7	6.83 – 7.07; 4	6.76 – 7.03; 4	
pH2 (range; n)		6.71 – 6.88; 7	6.67 – 6.85; 4	6.61 – 6.89; 4	
k_{PCr} (min^{-1})	10	0.44 ± 0.26	0.50 ± 0.37	1.50 ± 0.57	<0.001
V_{PCr} (mM min^{-1})	10	5.2 ± 3.1	9.4 ± 8.3	23.3 ± 8.9	<0.001
Group intermittent exercise – Subjects 16-20					
^{31}P MRS:					
PCr depletion (%)	5	44 ± 3	46 ± 3	38 ± 3	0.068
pH_{endex}	5	6.64 ± 0.21	6.65 ± 0.24	6.81 ± 0.20	0.138
pH1 (range; n)		6.99; 1	6.96 – 7.03; 2	6.79 – 7.02; 3	
pH2 (range; n)		6.79; 1	6.77 – 6.86; 2	6.63 – 6.80; 3	
k_{PCr} (min^{-1})	5	0.70 ± 0.65	0.68 ± 0.48	1.66 ± 1.00	0.043
V_{PCr} (mM min^{-1})	5	8.7 ± 8.1	9.2 ± 6.2	22.2 ± 14.2	0.043

Group ^{1}H MRS in Rest – Subjects 21-26				
Carnosine ($x10^{-6}$)*	6	1.74 ± 0.42	1.71 ± 0.48	0.884

CSA = cross-sectional area. Data are presented as mean ± standard deviations. *reflects the carnosine signal relative to water.

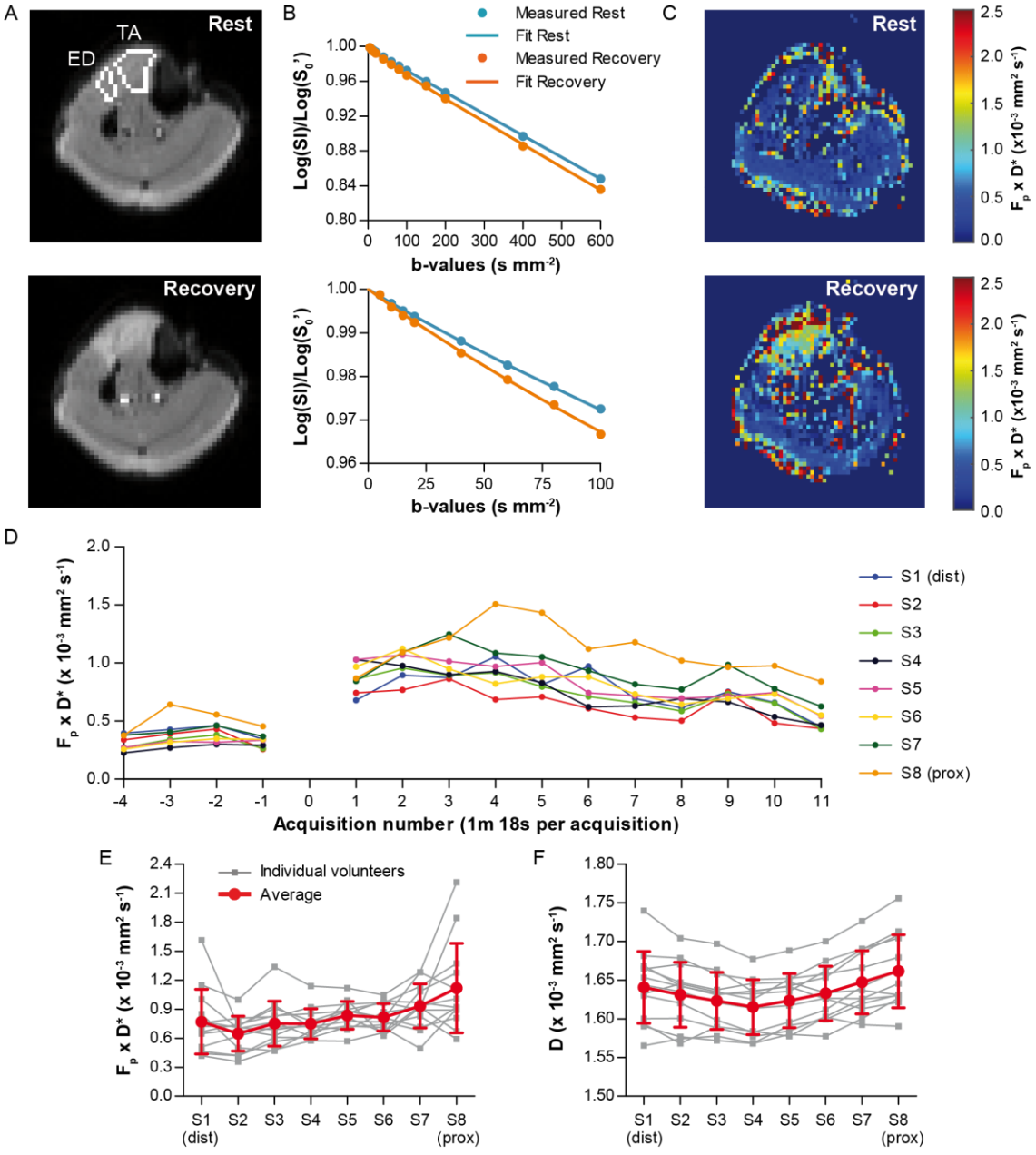

816

817 **Figure 3:** Results of IVIM acquisition of the lower leg for a typical example (A-D) and average
818 results in all volunteers (E/F). A) Diffusion weighted images at rest (top) and recovery (bottom,
819 acquisition 6) of the middle slice (S5) for b = 5 s mm^{-2} with the tibialis anterior (TA) and
820 extensor digitorum (ED) delineated. The TA and ED show an increased signal intensity after
821 exercise. B) Example fit of the IVIM model on data from the TA during rest (blue) and recovery
822 (orange) for b_0 to b_{600} (top) and b_0 to b_{100} (bottom). C) Blood flow related parameter F_pxD* map
823 during rest (top) and recovery (bottom, acquisition 6) indicating an increased blood flow in TA
824 and ED after exercise. D) $F_p \times D^*$ over time for the eight analyzed slices. Acquisition 0 is the first
825 acquisition after exercise and excluded from the analysis because it is prone to movement

826 artifacts. E-F) Average F_pxD* and diffusion coefficient (D) over all volunteers depicted as the
827 average over the whole recovery period after exercise (15 min 36 sec) for the eight slices (S1
828 distal, S8 proximal). Data are presented as mean ± SD.

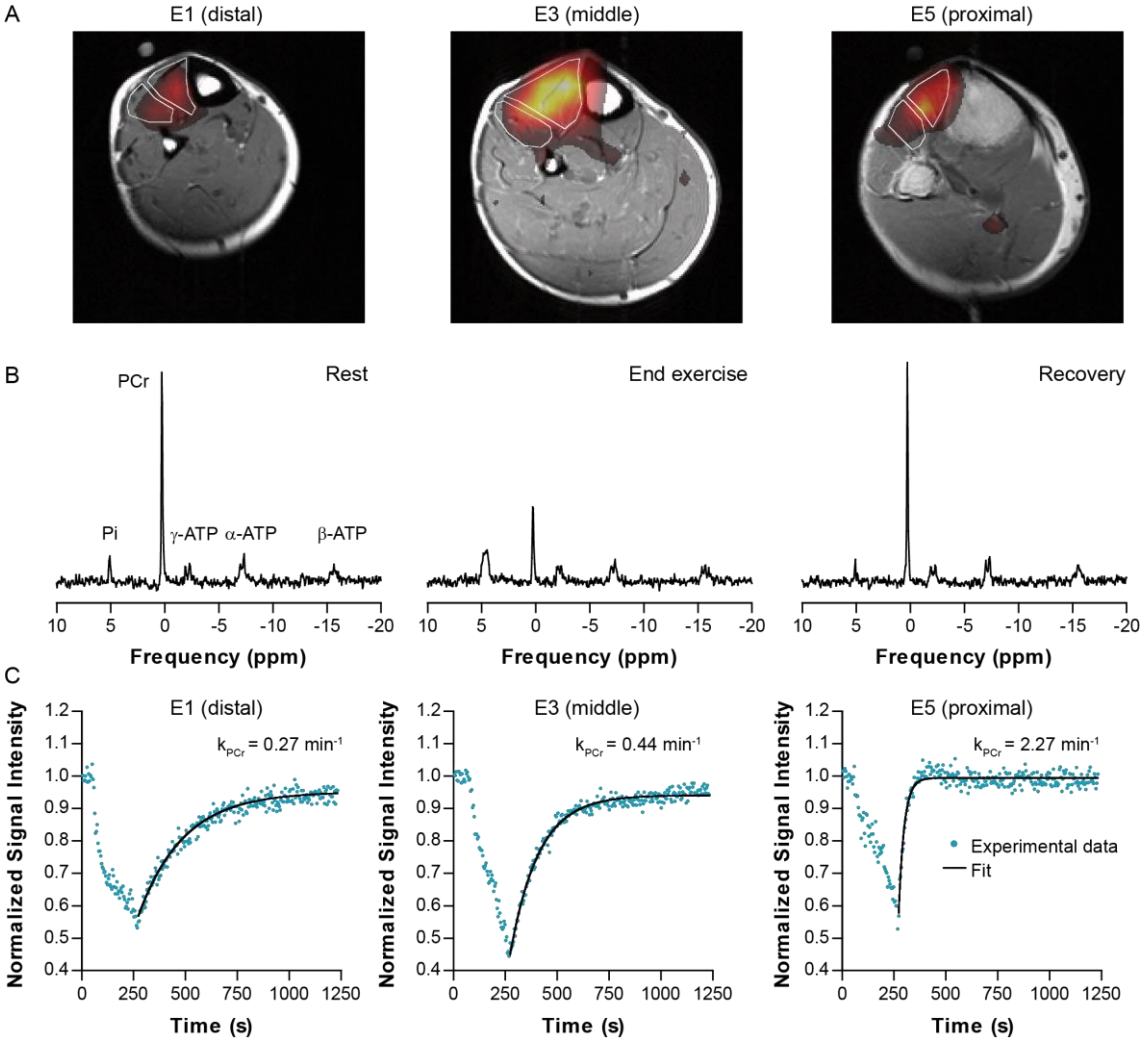

Figure 4. Example of ^{31}P imaging, ^{31}P spectra and PCr signal intensity time-course. A) Overlay of ^{31}P maps on T1 weighted ^{1}H images, indicating that the majority of the ^{31}P signal comes from the tibialis anterior. ^{31}P intensity variations between slices may also occur because of the ^{31}P slice profile. B) ^{31}P spectra showing inorganic phosphate (Pi), phosphocreatine (PCr) and the three resonances of ATP, and their change from rest to end-exercise to end-recovery. C) PCr signal time-course for coil elements E1 (distal), E3 and E5 (proximal), showing a faster PCr recovery proximally. The PCr recovery rate k_{PCr} assessed from spectra of each coil element is indicated.

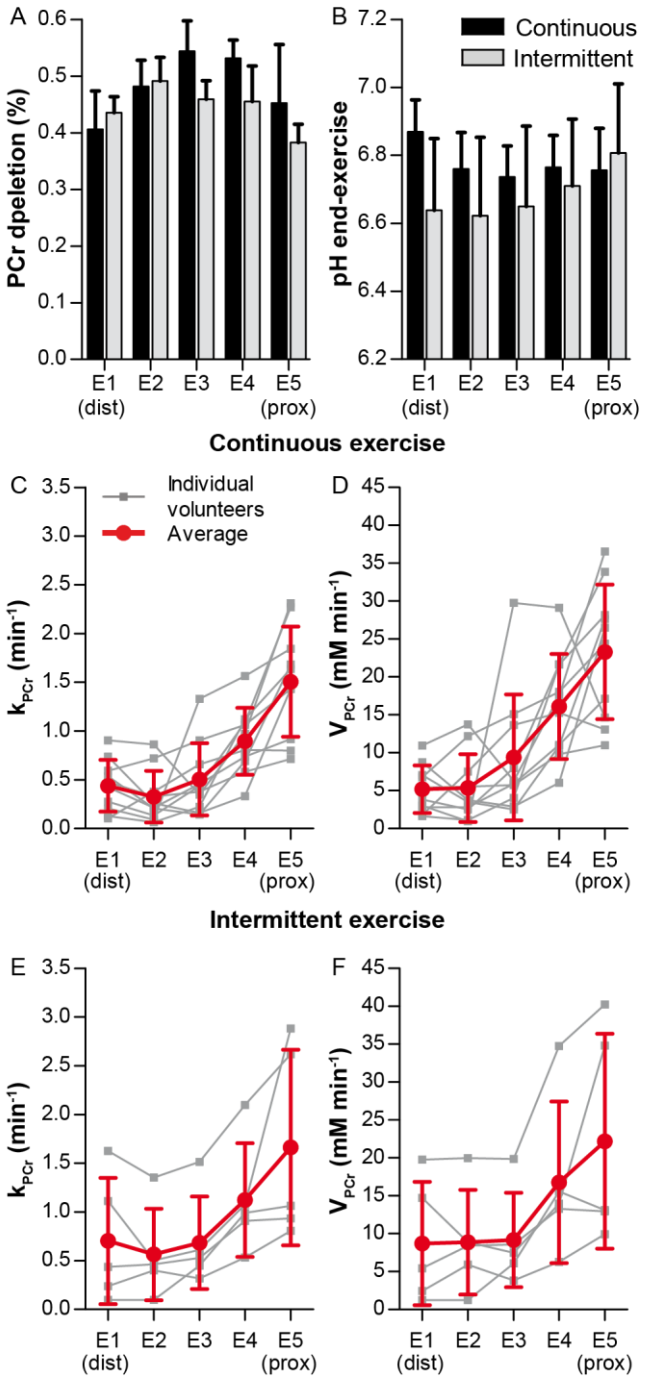

838

839 **Figure 5:** ^{31}P MRS results of the continuous isometric exercise and the intermittent isometric
840 exercise for the coil elements E1 (distal) to E5 (proximal). A) PCr depletion for both exercise
841 regimes. B) pH at end-exercise (pH_{endex}) for both exercise regimes. C) Phosphocreatine
842 recovery rate (k_{PCr}) during continuous isometric exercise. D) Estimated PCr resynthesis rate
843 (V_{PCr} = k_{PCr}×ΔPCr) during continuous isometric exercise. E) k_{PCr} during intermittent isometric
844 exercise. F) V_{PCr} during intermittent isometric exercise. Data are presented as mean ± SD.

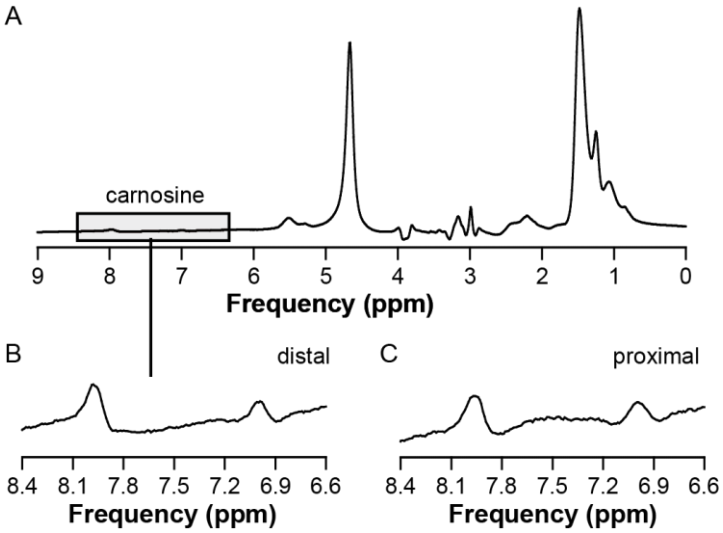

845

846 **Figure 6:** A) Example ^{1}H MR spectra from tibialis anterior. (A) Carnosine is represented by two
847 peaks, at 7 and 8 ppm. Expansions of this spectral region from spectra of voxels positioned (B)
848 distally and (C) proximally.

849

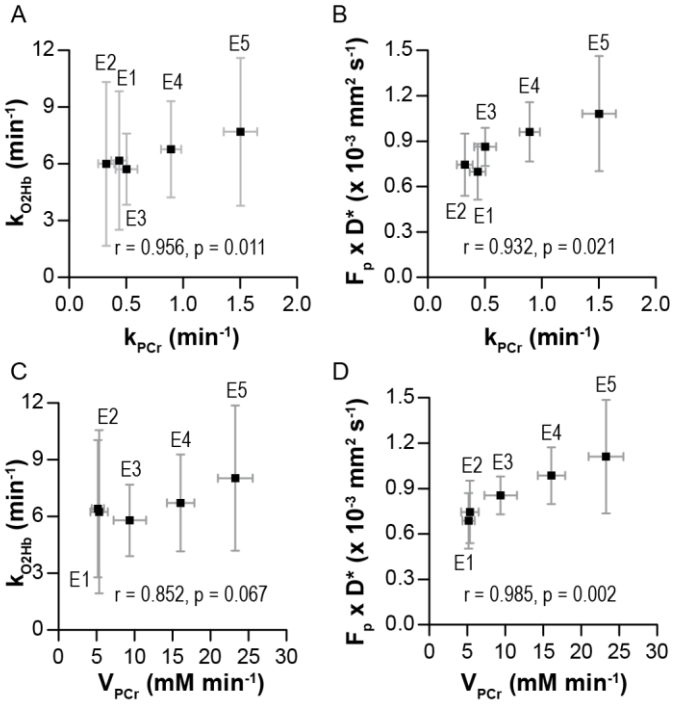

850

851 **Figure 7:** Phosphocreatine (PCr) recovery rate constant (k_{PCr}) and PCr resynthesis rate (V_{PCr})
852 displayed against the oxyhemoglobin recovery rate constant (k_{O2Hb}) and IVIM measured blood
853 flow (F_pxD*). Data are displayed per coil element as the average over all volunteers in mean ±
854 SD.

Table 3: Estimates of the (non-)linear mixed models and the corresponding p-values.

	BIC		**Estimates of the (non-)linear mixed model**				***p*-values**		
	Linear mixed model	Non-linear mixed model	β_0 *(Intercept)*	β_1 *(location)*	β_2 *(Location^2)*	β_3 *(pH_{endex})*	β_1 *(location)*	β_2 *(Location^2)*	β_3 *(pH_{endex})*
NIRS									
k_{O2Hb}	492	494	4.75 (0.85)	0.37 (0.09)			< 0.001		
IVIM									
D	-460	-503	1.66 (0.01)	-0.020 (0.003)	0.003 (0.0003)		< 0.001	< 0.001	
$F_p \times D^*$	8	4	0.80 (0.09)	-0.07 (0.04)	0.013 (0.004)		0.087	0.003	
^{31}P MRS									
PCr/Pi	137	138	6.8 (0.35)	0.44 (0.06)			<0.001		
k_{PCr}	292	291	-4.3 (3.9)	-0.37 (0.19)	0.11 (0.031)	0.72 (0.56)	0.060	0.001	0.207
pH_{endex}	-71	-74	6.97 (0.06)	-0.13 (0.04)	0.018 (0.006)		0.002	0.008	
PCr depletion	-99	-120	0.25 (0.04)	0.18 (0.03)	-0.027 (0.005)		<0.001	< 0.001	
V_{PCr}	348	347	6.2 (4.2)	-2.5 (3.2)	1.20 (0.52)		0.444	0.028	

According to the Bayesian Information Criterion (BIC), the k_{O2Hb} and PCr/Pi were best fitted with a linear mixed model and D, $F_p \times D^*$, k_{PCr}, pH_{endex}, PCr depletion, and V_{PCr} were best fitted with a non-linear mixed model. In case of k_{PCr}, pH_{endex} was also added as a fixed covariate. $p < 0.05$ indicates that the predictor (location, location^2, or pH_{endex}) has a significant effect on the fitted outcome measure (using type III F-test). Data are presented as mean (standard error).